

Fueling processes on (sub-)kpc scales

Francoise Combes

Observatoire de Paris, LERMA, Collège de France, CNRS, PSL University, Sorbonne University, 75014, Paris
e-mail: francoise.combes@obspm.fr

Abstract: Since the 1970s, astronomers have struggled with the issue of how matter can be accreted to promote black hole growth. While low-angular-momentum stars may be devoured by the black hole, they are not a sustainable source of fuel. Gas, which could potentially provide an abundant fuel source, presents another challenge due to its enormous angular momentum. While viscous torques are not significant, gas is subject to gravity torques from non-axisymmetric potentials such as bars and spirals. Primary bars can exchange angular momentum with the gas inside corotation, driving it inward spiraling until the inner Lindblad resonance is reached. An embedded nuclear bar can then take over. As the gas reaches the black hole's sphere of influence, the torque turns negative, fueling the center. Dynamical friction also accelerates the infall of gas clouds closer to the nucleus. However, due to the Eddington limit, growing a black hole from a stellar-mass seed is a slow process. The existence of very massive black holes in the early universe remains a puzzle that could potentially be solved through direct collapse of massive clouds into black holes or super-Eddington accretion.

Keywords: galaxies: active nuclei; galaxies: bars; spirals; black holes; angular momentum; molecular torus; fueling; feedback; warps

1 Introduction

One of the main issues to explain the fueling of active galactic nuclei (AGN) is the mechanism to get rid of the angular momentum (AM). The black hole may swallow the neighbouring stars, which will create a depletion among those with a low AM. It will require a long relaxation time to replenish this loss cone, so that the fueling will rely on the gas infall. The latter requires gravity torques, tangential forces, and therefore non axisymmetric features, such as bars or spirals. Large-scale features are not sufficient, and should be supported by embedded bars to prolong their action towards the center.

The high spatial resolution provided by the ALMA interferometer has been able to reveal these embedded structures, in particular nuclear spirals inside the nuclear rings, corresponding to the inner Lindblad resonance (ILR) of the bars. Examples of these structures have been unveiled in nearby Seyfert galaxies.

Inside these nuclear spirals, at 10 pc scale, molecular tori have been unveiled, as circumnuclear disks, kinematically decoupled from the large-scale disk. The origin of the decoupling may be found in several causes, like accretion of gas with different AM, and/or precession and warping of the very central disk due to relativistic effects, coupled with the supermassive black hole spin.

2 Angular Momentum Problem

The problem comes from the large contrast between the angular momentum of the gas in the last stable orbit, $L = 2 \times 10^{24} (M/10^8 M_\odot) \text{ cm}^2/\text{s}$, for a typical black hole mass of $10^8 M_\odot$, and the gas AM at 3 kpc, $L = 10^{29} \text{ cm}^2/\text{s}$. The ratio of these two values means that the gas has to lose 5 orders of magnitude in AM, in a relatively short dynamical time. The illustration of the AM increase with radius is shown in Fig. 1. For a typical luminosity of 10^{46} erg/s , the central engine has to swallow $2 M_\odot/\text{yr}$, during a duty cycle of 100 Myr.

Stars with low AM in the neighborhood of the black hole can be tidally sheared, and their gas be accreted in a rotating disk. These TDE (Tidal Disruption Event) may occur at the frequency of one every 10 000 yrs in the Milky Way. Some have been detected in external galaxies, their signature being a characteristic light curve decreasing with time as a $-5/3$ power-law (Miller et al. 2015). But soon, the depletion and loss cone effect dries up this fueling source, unless galaxy interactions re-shuffled the stellar distribution, and creates nuclear star clusters, in a nuclear starburst.

Gas is however the main fuel, and is driven inwards through non-axisymmetries of the galaxy potential. Several steps can be distinguished in this process. First, primary bars of typical diameters 10 kpc, can drive the gas from their corotation to $R \sim 100 \text{ pc}$, where the gas may be stalled in a ring. Then embedded nuclear bars can prolong their action from 100 pc to 10 pc. Non-axisymmetries are mainly of $m=2$ morphology, but also $m=1$ (lopsidedness), or tidal forces from companions can play a role.

At smaller scales of 1-10 pc, other processes also have to be considered: turbulence, viscosity, warps, bends, dynamical friction, formation of thick disks, as long as gas remains in sufficient amount.

2.1 Dynamics of bars

Let us recall the main features of barred galaxies: the stellar orbits are classified through a skeleton of periodic orbits. The latter are orbits that close on themselves after one or more turns in the bar rotating frame. They are the building blocks which determine the stellar distribution function, since they define families of trapped orbits around them. Trapped orbits are non-periodic, but oscillate about one periodic orbit, with a similar shape. The periodic orbits are numerous (see the review by Contopoulos & Grosbøl (1989)), let us mention here the most important ones for the bar support. Inside corotation, the x1 family is the main family supporting the bar. Orbits are elongated parallel to the bar, within corotation. There exists also the x2 family, but only between the two inner Lindblad resonances (ILR), if they exist. They are more round, and elongated perpendicular to the bar. The existence of two ILR's in the axisymmetric sense might not be sufficient for the x2 family to appear. When the bar is strong enough, the x2 orbits disappear. The bar strength necessary to eliminate the x2 family depends on the pattern speed, the lower this speed, the stronger the bar must be. Outside corotation, the 2 / 1 orbits that are run in the retrograde sense in the rotating frame are perpendicular to the bar inside the outer Lindblad resonance (OLR), and parallel to the bar slightly outside (see discussion by Kalnajs (1991)). Their shape reveals a characteristic figure-eight, that is very similar to the dimpled shape of some outer rings in barred galaxies.

In summary, periodic orbits are aligned parallel or perpendicular to the bar, and their orientation changes by 90° at each resonance (Contopoulos & Papayannopoulos 1980; Athanassoula 1992). Gas tends to follow periodic orbits, but its dissipative character, due to cloud collisions, means that orbits cannot cross. Instead their orbits are tilted, and they change gradually by 90° at each resonance. The crowding of these stream lines produces a spiral morphology (Sanders & Huntley 1976). The spiral is open, and at maximum can rotate by $180-360^\circ$.

2.2 Embedded structures

Because the gas and the stars are not in phase, stellar bars exert a torque on the gas, except at resonances, where the gas piles up and stalls in rings, aligned with the bar in some way. When mass has been accumulating in the center, all frequencies Ω and $\Omega - \kappa/2$, the orbit precessing rate, see their value significantly increased, implying the existence of two ILR. In between these, the periodic orbits (x2) are perpendicular to the bar. Stars cannot sustain the bar anymore, and weaken it. The z-resonance, creating peanut-shape bulges, also weakens the bar. This triggers the decoupling of a second bar, an embedded nuclear bar (Friedli & Martinet 1993). This second bar rotates faster than the primary bar, and both are misaligned (Buta & Combes 1996).

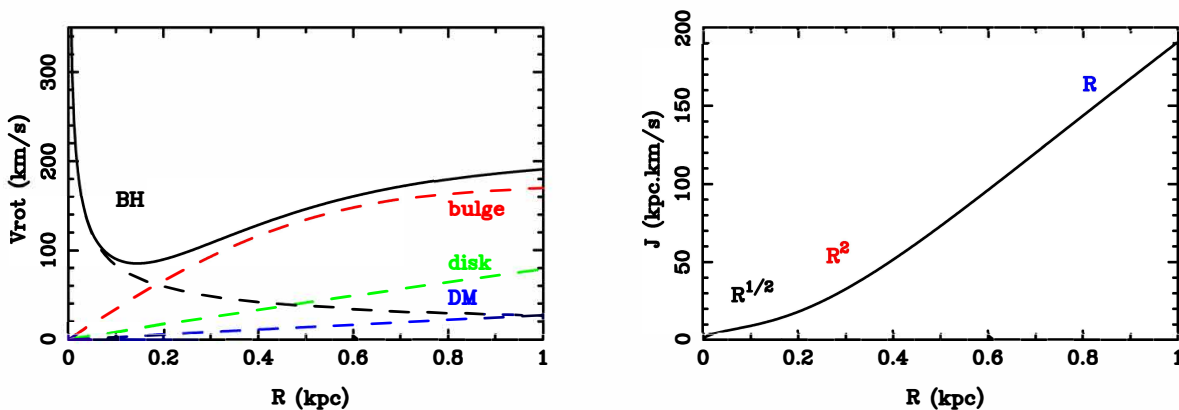


Figure 1: How does the angular momentum increase with radius around a super-massive black hole (BH)?: **left**, the typical rotation curve in a spiral galaxy is dominated by the BH mass in the center (keplerian potential), then is rising due to the bulge, and finally ends as flat due to the conspiracy of the disk and dark matter halo (DM). These various contributions are marked in different colors; **right**, the corresponding angular momentum per unit mass increases as power-laws of the radius, with slopes first one-half (Keplerian), than two and one.

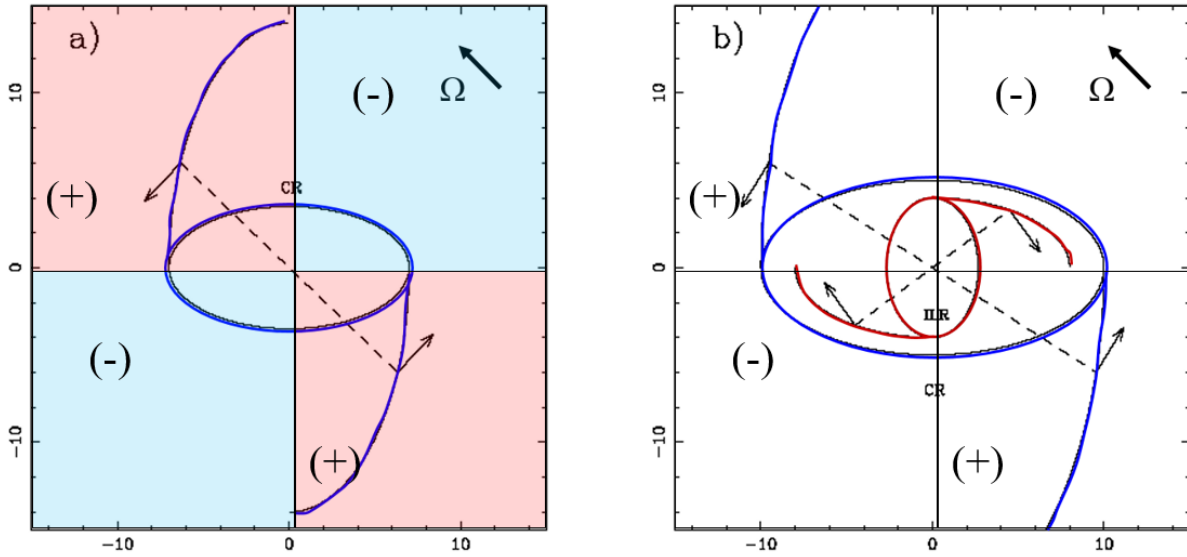


Figure 2: The sign of the torques exerted by the bar on the gas can be obtained geometrically through these schematic diagrams: **left**, outside corotation, or roughly outside the bar, the torque is positive (red quadrant) with respect to the sense of rotation (Ω), and the gas is driven out toward the outer Lindblad resonance (OLR); **right**, inside the corotation, the torque is negative (blue quadrant), and the gas is driven inward, down to the inner resonance (ILR).

2.3 Fueling AGN: removing angular momentum (AM)

The torques exerted on the gas by the bar change sign at each resonance, cf Fig. 2. Outside the corotation radius (CR), the gas is driven outwards and accumulates at the outer Lindblad resonance (OLR). Inside CR, the gas is driven inwards, at least down to ILR. To quantify the phenomenon, bar gravity torques can be computed from the red images tracing old stars, and the potential. When the gas distribution is overlaid on the torque map (cf Fig. 3), the sign and amount of the gas infall can be estimated, as in NGC3627 (Casasola et al. 2011). The correlation between bars and AGN is still debated (Schawinski et al. 2010; Masters et al. 2011; Cardamone et al. 2011; Alonso et al. 2014), since the time-scales corresponding to the primary and secondary bars are quite different, and also different from the AGN duty cycle.

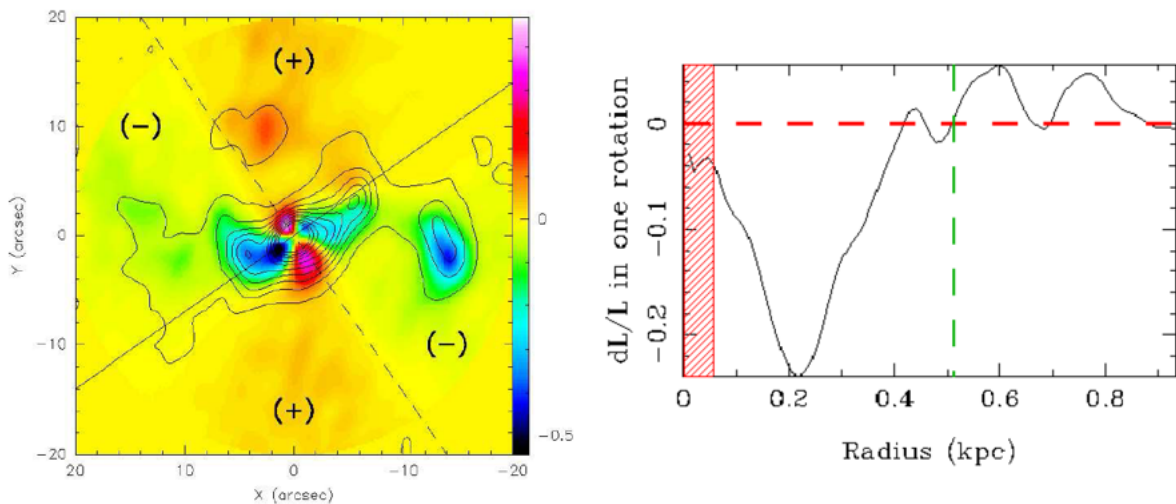


Figure 3: The gravity torques can be measured on real galaxies, by computing in each pixel the potential and forces from a red image (old stars), and comparing with the observed gas density. The **left** image is the torque map in color, with the bar splitting the plane in four quadrants, for NGC 3627. The gas density is overlaid in contours. The **right** plot quantifies the relative angular momentum lost in one rotation, while averaging the torque over azimuth, weighted by gas density. Adapted from Casasola et al. (2011).

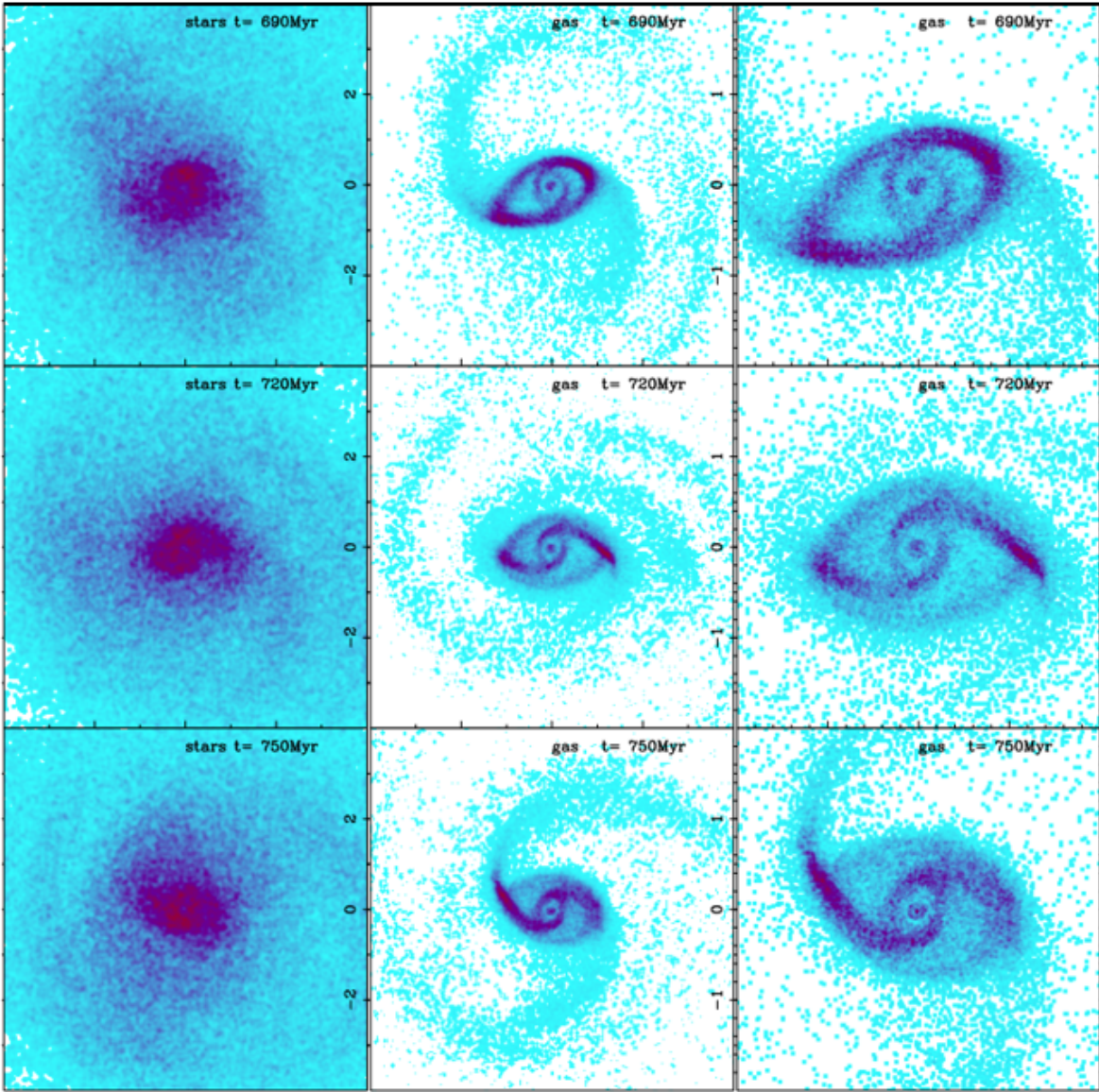


Figure 4: Hydro-N-body simulation of a double bar in a spiral galaxy. The **left** panel shows the stellar component surface density (linear scale, axes in kpc), the **middle** panel shows the gas component (log scale), while the **right** panel is also the gas, in a zoomed spatial scale. The simulation shows clearly that the gas first piles up in the external ring (ILR of the primary bar), then progressively infalls inside the ILR to gather at the nuclear bar resonance. Adapted from Hunt et al. (2008).

During a survey of about 20 galaxies with the IRAM interferometer, statistics of fueling at the 10-100 pc scale was obtained (García-Burillo & Combes 2012). Only 35% of negative torques were measured in the center, the rest of the times, positive torques were measured, or gas was stalled in a ring. In this case, future fueling has to wait for the decoupling of a secondary bar, as shown in the simulation of Fig. 4. This means that the fueling phases are short, a few 10^7 yrs, and may be due to feedback. Star formation is also fueled by the torques, and is always associated with AGN activity, but with longer time-scales.

3 Small-scale fueling with ALMA

With the advent of ALMA, higher spatial resolution is possible, to explore the 10 pc scales in nearby galaxies. One of the first barred spiral observed was NGC 1433 (cf Fig. 5). While only a star forming ring was observed at ILR with HST, a second ring was detected in the molecular gas with ALMA, corresponding to the second ILR. The computation of the torques have shown that the AGN is not presently fueled, but positive torques bring the gas from

the center to the second ring. Negative torques outside this second ring contribute to accumulate gas there (Smajić et al. 2014). On the minor axis, an outflow has been detected, with small velocity. It is one of the smallest outflows detected, with $M(\text{H}_2) = 3.6 \times 10^6 M_\odot$ and a flow rate of $7 M_\odot/\text{yr}$ (Combes et al. 2013).



Figure 5: HST image of NGC1433 bar, with characteristic leading dust lanes, ending down to a blue ring at the inner Lindblad resonance (ILR). The insert displays the blue ring from HST overlaid with the orange-red image from ALMA of the molecular gas, traced by its CO(3-2) emission. The latter reveals a second ring inside the first ILR. Adapted from Combes et al. (2013).

Other barred Seyfert galaxies, like NGC1566 were found in the feeding phase (cf Fig. 6). Inside the ILR ring, the CO(3-2) emission map from ALMA reveals the existence of a nuclear disk, with a trailing nuclear bar. The existence of the trailing spiral was a surprise, since without the gravitational influence of the central black hole, a leading spiral is expected. This is due to the shape of the $\Omega - \kappa/2$ curve as a function of radius. When the gas infalls, it precesses more rapidly if the curve is climbing when radius is reduced, which means a trailing arm, and the contrary if the curve declines, cf Fig. 7. If the spiral is trailing, it means that the gas feels a climbing curve, due to the BH, and it has entered the sphere of influence of the BH. The computation of the torques in NGC1566 has confirmed the evidence of fueling (Combes et al. 2014).

In several other barred galaxies, a trailing nuclear spiral has been revealed in the molecular component with ALMA, for instance in NGC 1808 or NGC 613. This indicates that the gas has entered the sphere of influence of the black hole, making the torque negative, ensuring the fueling of the AGN. This trailing spiral develops always inside the ILR ring of the bar (Audibert et al. 2021).

NGC 613 is the academic case of a strong barred galaxy, with a star forming gas ring at ILR. The first ALMA observations, with moderate spatial resolution, could see only the ring, without resolving the internal structure (Miyamoto et al. 2017). With a beam of 60mas, it was possible to clearly see an internal trailing nuclear spiral, and inside the spiral a molecular torus (cf Fig. 8). The computation of the torques indicates that the gas can lose all its

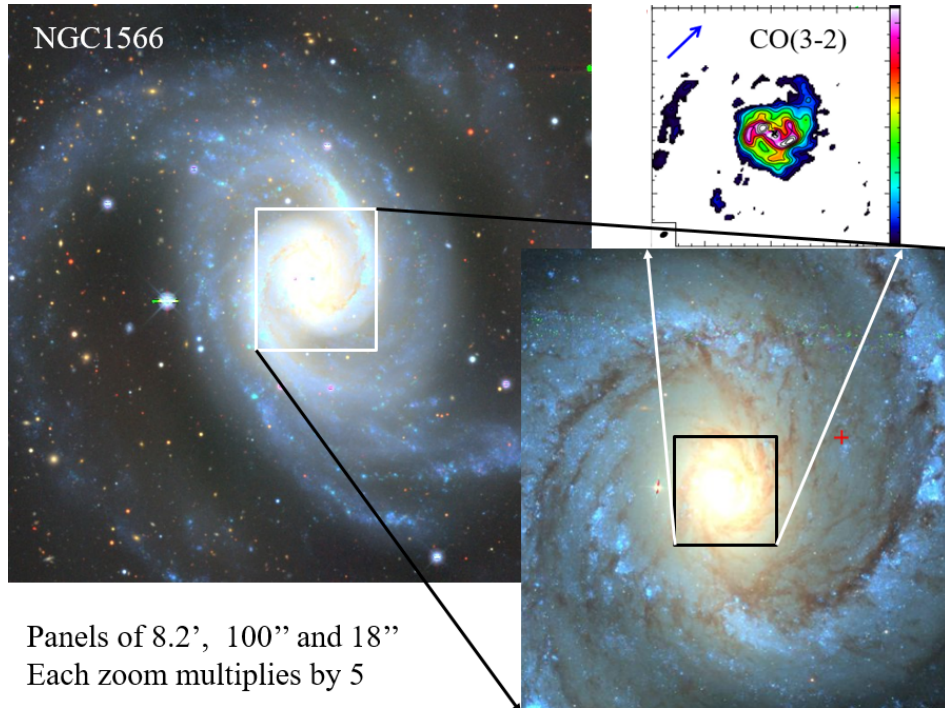


Figure 6: The barred spiral galaxy NGC 1566 reveals several embedded structures, as seen in these three progressively zoomed images. The last one reveals a trailing nuclear spiral in the molecular gas, traced by its CO(3-2) emission observed with ALMA. Adapted from Combes et al. (2014).

angular momentum in only one rotation, when inside 50 pc radius (Audibert et al. 2019). In addition, a molecular outflow is detected along the minor axis, parallel to the cm-wave detected radio jet.

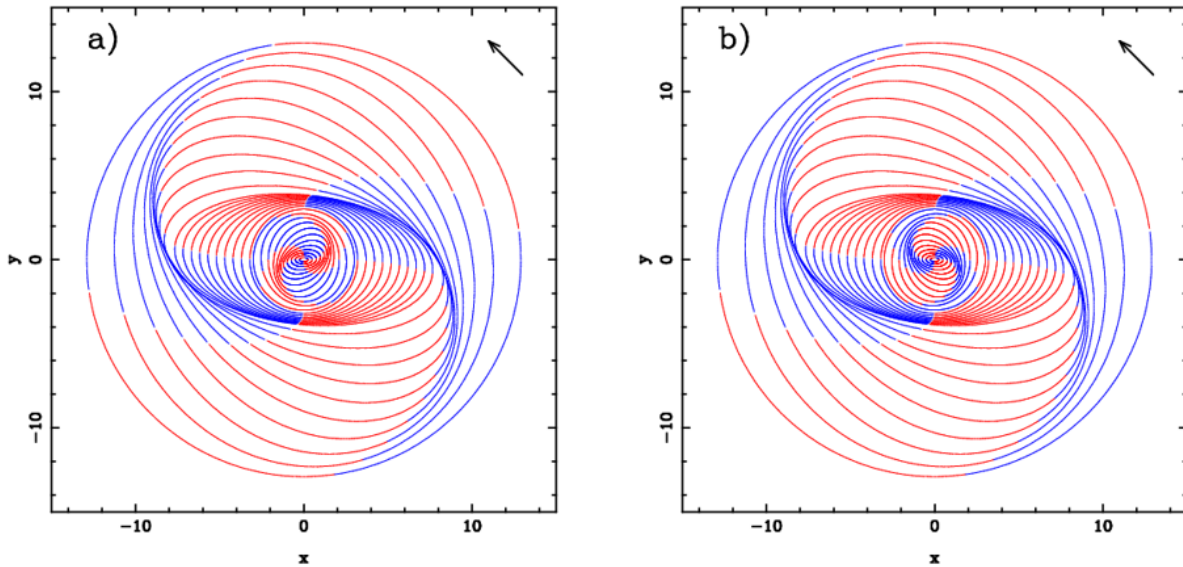


Figure 7: Gas streamlines schematically represented by elliptical orbits, precessed to form logarithmic spirals. They are initially aligned on the horizontal axis (parallel to the bar) and colored according to the four quadrants. The pattern speed is such that there exists an ILR inside the bar, delineated by a ring. **Left:** without a super-massive black hole (BH), the precessing rate decreases towards the center, and the gas forms a leading nuclear spiral. **Right:** with a BH dominating the potential inside the ILR, the precessing rate increases towards the center, and the gas forms a trailing spiral. This changes the sign of the torque exerted on the gas.

4 Molecular tori

Our vision of the central regions of AGN surrounding the black hole have changed significantly in the recent years. For a long time, around the accretion disk and the broad line region (BLR), a dusty torus, with a donut shape was assumed to exist. It was thought to obscure the BLR for observers seeing the accretion disk almost edge-on. But infrared interferometers have shown that the dust is frequently detected in the polar direction, instead of being aligned along the putative torus. This polar dust must be ejected through the AGN wind, starting from the dust sublimation radius (pc size), and forming the border of a hollow cone (Hönig 2019). The gas motion is then both infall in a thin disk, forming a molecular torus, and then outflow in the perpendicular direction.

Figure 8 shows that the molecular torus, inserted in the nuclear spiral, has a decoupled kinematics, i.e. the kinematic major axis is not aligned with that of the large-scale disk (Combes et al. 2019; Audibert et al. 2019).

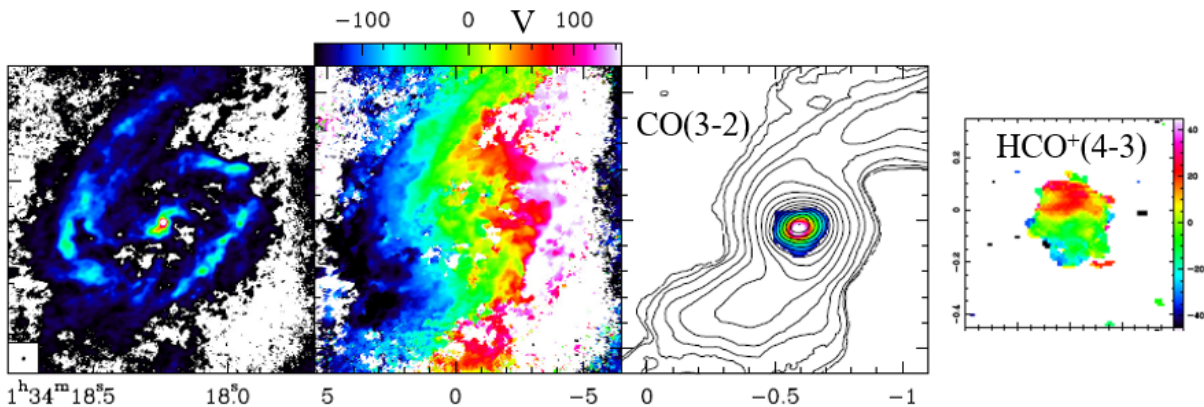


Figure 8: The barred galaxy NGC 613 shows a contrasted ring at its ILR, in the molecular gas traced by CO(3-2) with ALMA. From left to right is the gas surface density, then the velocity field, and a 10-fold zoom of the gas density (contours), with the radio continuum (color-scale) at the center. The right-most panel is the velocity field of HCO⁺(4-3) emission, revealing a misalignment with the large-scale gas. Adapted from Combes et al. (2019) and Audibert et al. (2019).

This misalignment is frequent in all nearby galaxies observed with ALMA with 10 pc resolution, such as NGC 1672 or NGC 1326 in the NUGA sample (Combes et al. 2019), or NGC 5643, NGC 6300 in the GATOS sample (García-Burillo et al. 2021). It is yet not possible to determine whether the central molecular torus is simply continuously warped, or tilted, with discontinuous disks torn into a few pieces. Circinus is one of the nearest galaxies, observed down to 2 pc resolution, and shows a nuclear spiral, of 20-30 pc, with inside another circum-nuclear disk, which can be interpreted as the molecular torus. It is self-absorbed in CO(3-2) but not in CO(6-5), nor in the dense gas tracers, such as HCO⁺. In addition to this cold thin disk, fueling the AGN, there is an outflow in the polar direction, composed of warm dust and ionized gas, cf Fig. 9 (Izumi et al. 2018; Tristram et al. 2022).

The prototypical Seyfert 2 NGC 1068 has been intensively observed, with high resolution at many-wavelengths. While the near-infrared reveals clearly the hollow polar cone in warm dust (Gratadour et al. 2015), the cold component in the millimeter domain reveals a molecular torus of 7-10 pc in diameter (García-Burillo et al. 2016; Imanishi et al. 2020). The torus is quasi edge-on, misaligned with the large-scale disk, warped, more inclined than the water maser disk, and maybe suffers from counter-rotation (Impellizzeri et al. 2019; Imanishi et al. 2020). In contrast, the barred Seyfert 1 galaxy NGC 1097, with ALMA at 10 pc resolution, does not show any dense and compact torus. There is a nuclear spiral inside the star-forming ring at the ILR of the bar (Fathi et al. 2006; Izumi et al. 2017). The absence of torus concerns about 10-20% of low-luminosity AGN. This percentage increases with the Eddington ratio, and could be related to the AGN feedback (García-Burillo et al. 2021).

The influence of the AGN activity is indeed visible on the molecular gas concentration. The latter can be quantified by the surface density ratio of the molecular gas inside 50 pc and inside 200 pc. The most active AGN have less H₂ concentration. The latter drops for X-ray luminosities $L_x > 10^{42.5}$ erg/s, or for Eddington ratios $> 10^{-3}$, see Fig. 10, (García-Burillo et al. 2021).

5 Early black holes

Along their life-time, galaxies grow both their bulge and their black hole, in synergy, so that a tight relation can be observed between both masses (Kormendy & Ho 2013). Secular evolution, together with some tidal interaction with companions, can provide the fuel for AGN and BH growth. However, AGN feedback makes the BH growth intermittent, as described above. Some different processes should occur at high redshift, to account for the observations of high black hole masses ($M > 10^9 M_{\odot}$) already at $z > 6$ (Venemans et al. 2016). Hundreds of quasars have been detected at high redshift, $z > 6$, with black hole masses between 10^8 and $10^{10} M_{\odot}$, in the first billion years of the Universe (e.g. Mortlock et al. 2011; Yang et al. 2020; Farina et al. 2022). The black hole growth rate through accretion is proportional to its mass, and is thus very slow at the beginning, starting with stellar mass seeds. At any time, the Eddington luminosity imposes an upper limit in the accretion rate, limit which is proportional to the BH mass. In contrast, at high redshift, black holes appear to grow faster than their host bulges, and the proportionality relation breaks. Several solutions have been proposed. One is to assume that the BH in the early times accrete exceptionally faster than their Eddington rate, and this without being stopped by AGN feedback. Simulations of black hole growth with super-Eddington accretion, even in a massive over-density environment, progenitor of a cluster, in general do not succeed to reproduce the observed massive black holes at $z=6$ (Sassano et al. 2023), nor explain why the black hole growth is more rapid than the stellar mass growth, contrary to what is observed at $z=0$. However, with some modifications of the usual scenario, taking into account less efficient AGN feedback, more efficient accretion, and starting earlier with a more massive seed, it is possible to account for the observations (Bennett et al. 2024).

An alternative solution is to assume that the BH collapses directly from a massive cloud, due to primordial metal abundance, and lack of fragmentation. The seeds to form the first black holes would then be much more massive than stellar, and the growth rate would be strong since the start. This however assumes contrived suppression of H_2 molecule formation, and remains debated.

The existence of intermediate mass black hole (IMBH) is part of the puzzle, since they have not yet been detected unambiguously. The direct collapse scenario could explain their low abundance. The major challenge for observations of IMBHs is their small mass and small impact in their surroundings. Since the radius of influence of a black hole scales linearly with its mass, it requires very high spatial resolution, to detect their impact on the gas or stellar component. Also the dynamical friction time-scale for a black hole to decay towards nuclei is inversely proportional to the mass, and IMBH might not have time to infall within a Hubble time (e.g. Di Matteo et al. 2023).

An promising way to detect IMBH is to search for AGN signatures, and candidates have been observed in several low-mass galaxies (Chilingarian et al. 2018). There exist candidates for IMBH in several dwarf active galaxy nuclei (e.g. Mezcuca 2017), however in the core of globular clusters, where they were expected, only a collection of stellar-mass black holes have been detected instead (Vital & Mamon 2021; Vital et al. 2023).

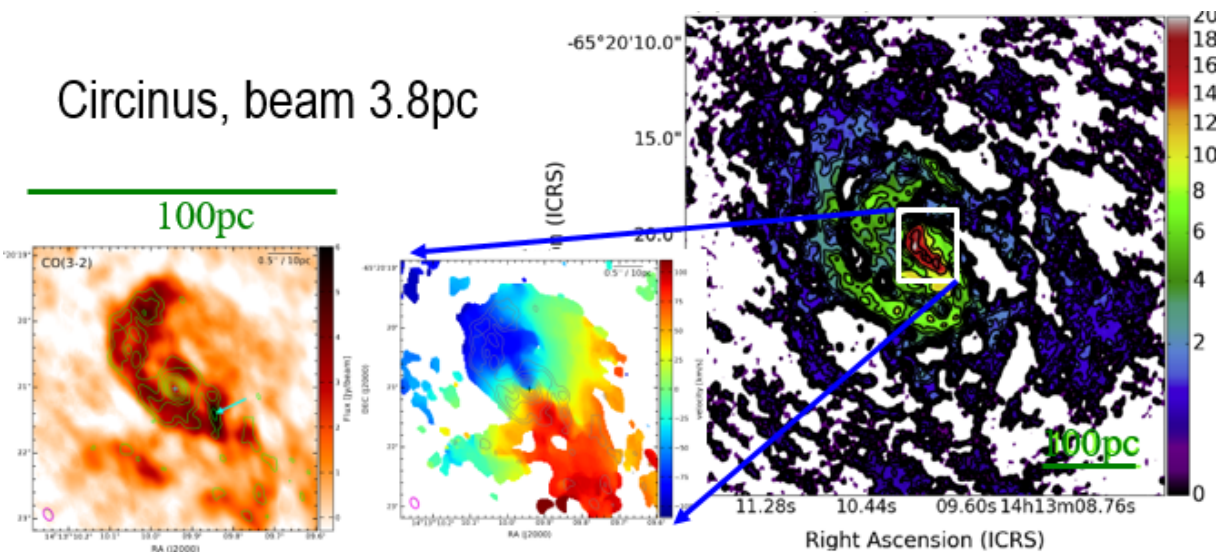


Figure 9: Image of the molecular gas, obtained in CO(3-2) with ALMA, of the Circinus galaxy, with a resolution of 3.8 pc. There is a nuclear spiral, of 20-30 pc, and inside another circum-nuclear disk, which could be the molecular torus (edge-on, for this type 2 AGN). Adapted from Tristram et al. (2022).

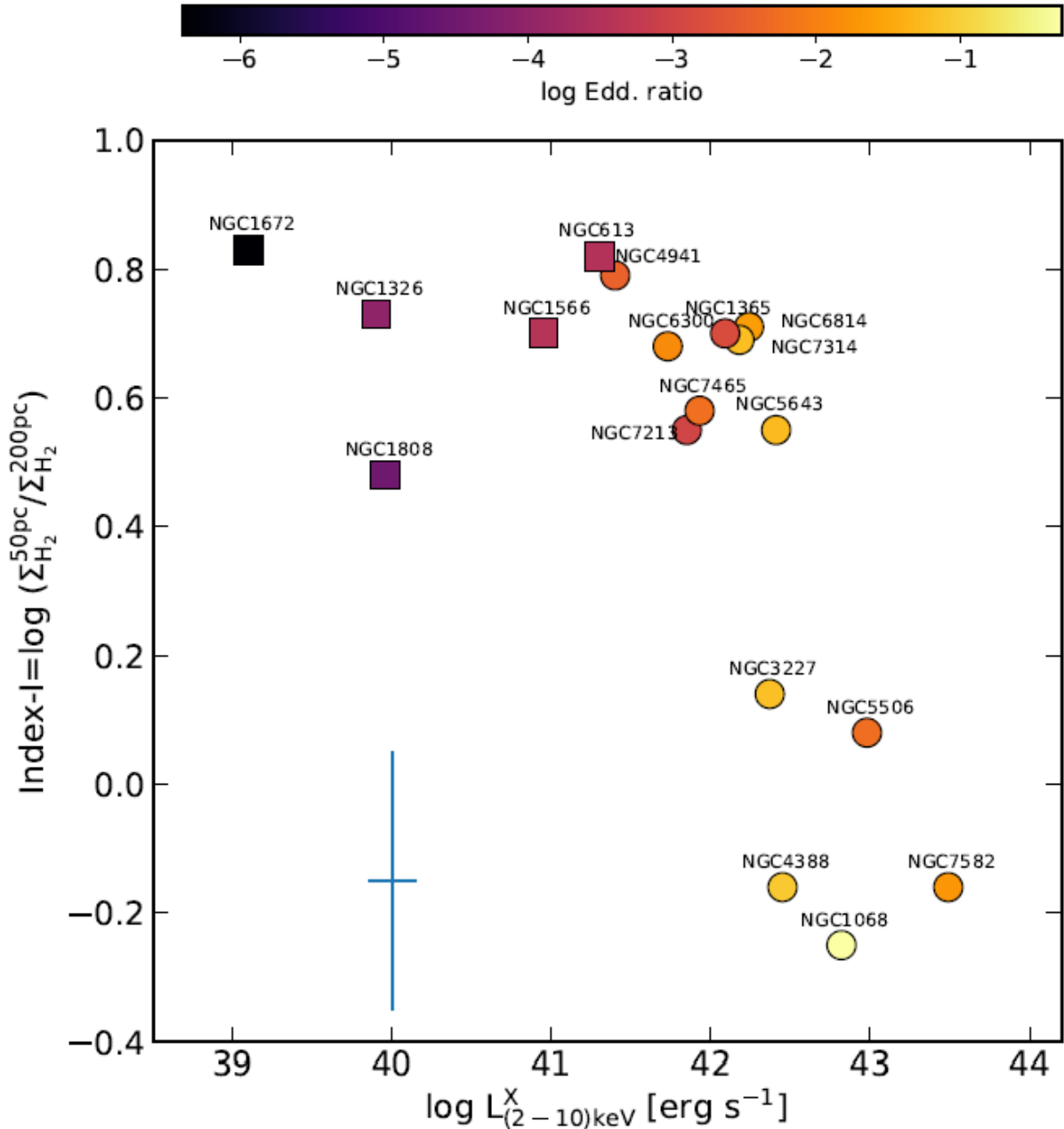


Figure 10: Concentration of molecular gas in the central regions of galaxies, versus their AGN luminosities measured in the 2–10 keV X-ray band. The concentration is measured from the ratio of the average H_2 surface densities at two spatial scales: $r < 50$ pc and $r < 200$ pc, characteristic of the nuclear and circumnuclear regions. Symbols are color-coded as a function of the Eddington ratios. The sample galaxies: NUGA (square markers) and GATOS (circle markers) can be separated both by their AGN activity, and molecular gas concentration. Adapted from García-Burillo et al. (2021).

6 Summary

The AGN fueling requires non-axisymmetries in the galaxy potential to drive the gas inwards. The primary bar in spiral galaxies can drive the gas from its corotation to the inner Lindblad resonance, where the gas is accumulating, and forms a starbursting ring, at the scale of 100 pc. Further fueling has to await the formation of a nuclear bar, embedded inside the ILR ring. ALMA has revealed 10 pc scale structures inside the ring, in particular trailing nuclear spirals, indicating that the gas has entered the sphere of influence of the central black hole. The stellar potential then prolongs the action of the primary bar to fuel the AGN. Inside the nuclear spiral a molecular disk, kinematically decoupled, is often found, that can be interpreted as the molecular torus.

The misalignment of the torus can be explained by gas accretion with different angular momentum. This occurs

naturally through star formation/supernovae feedback, which ejects gas above the plane. When this gas comes back, by the fountain effect, it can arrive in any direction with a random angular momentum. Numerical simulations have shown that even polar gas rings or disks can be formed (Renaud et al. 2015; Emsellem et al. 2015).

The decoupling of molecular tori is not too surprising, given the very different dynamical time-scales between the 10 pc and 100 pc scales. In addition, the material at much less than 1 pc from the black hole is certainly influenced by relativistic effects, related to the black hole spin: the Bardeen-Petterson effect, where the torque exerted by the BH tends to align the material perpendicular to its spin, and produces warps. Warping might also be radiation-driven (Pringle 1996; Maloney & Begelman 1997).

Contrary to the existence of a tight relation between bulge and black hole masses in nearby galaxies, super-massive black holes grow relatively faster than the stellar component in early galaxies, in the first billion year of the Universe. To reproduce this behavior, simulations have assumed super-Eddington accretion, and low-efficiency AGN feedback at these epochs. Alternatively, direct collapse of super-massive stars into black holes might contribute to the solution. Future observations in the early universe with JWST might enlighten the issue.

Acknowledgements: Thanks to Ilaria Ruffa and the organisers of the conference "AGN on the beach" in Tropea, Italy, where this material was discussed. FC has benefited from the support of the Programme National Cosmologie et Galaxies. Figures 3-6 and 8-10 are reproduced with permission from Astronomy & Astrophysics, © ESO.

References

- Alonso, S., Coldwell, G., & Lambas, D. G. 2014, *A&A*, 572, A86
- Athanassoula, E. 1992, *MNRAS*, 259, 328
- Audibert, A., Combes, F., García-Burillo, S., et al. 2019, *A&A*, 632, A33
- Audibert, A., Combes, F., García-Burillo, S., et al. 2021, *A&A*, 656, A60
- Bennett, J. S., Sijacki, D., Costa, T., Laporte, N., & Witten, C. 2024, *MNRAS*, 527, 1033
- Buta, R. & Combes, F. 1996, *Fund. Cosmic Phys.*, 17, 95
- Cardamone, C. N., Schawinski, K., Masters, K., Lintott, C., & Fortson, L. 2011, in *American Astronomical Society Meeting Abstracts*, Vol. 218, *American Astronomical Society Meeting Abstracts #218*, 206.03
- Casasola, V., Hunt, L. K., Combes, F., García-Burillo, S., & Neri, R. 2011, *A&A*, 527, A92
- Chilingarian, I. V., Katkov, I. Y., Zolotukhin, I. Y., et al. 2018, *ApJ*, 863, 1
- Combes, F., García-Burillo, S., Audibert, A., et al. 2019, *A&A*, 623, A79
- Combes, F., García-Burillo, S., Casasola, V., et al. 2013, *A&A*, 558, A124
- Combes, F., García-Burillo, S., Casasola, V., et al. 2014, *A&A*, 565, A97
- Contopoulos, G. & Grosbøl, P. 1989, *A&A Rev.*, 1, 261
- Contopoulos, G. & Papayannopoulos, T. 1980, *A&A*, 92, 33
- Di Matteo, T., Ni, Y., Chen, N., et al. 2023, *MNRAS*, 525, 1479
- Emsellem, E., Renaud, F., Bournaud, F., et al. 2015, *MNRAS*, 446, 2468
- Farina, E. P., Schindler, J.-T., Walter, F., et al. 2022, *ApJ*, 941, 106
- Fathi, K., Storchi-Bergmann, T., Riffel, R. A., et al. 2006, *ApJ*, 641, L25
- Friedli, D. & Martinet, L. 1993, *A&A*, 277, 27
- García-Burillo, S., Alonso-Herrero, A., Ramos Almeida, C., et al. 2021, *A&A*, 652, A98
- García-Burillo, S. & Combes, F. 2012, in *Journal of Physics Conference Series*, Vol. 372, *Journal of Physics Conference Series*, 012050
- García-Burillo, S., Combes, F., Ramos Almeida, C., et al. 2016, *ApJ*, 823, L12
- Gratadour, D., Rouan, D., Grosset, L., Boccaletti, A., & Clénet, Y. 2015, *A&A*, 581, L8
- Hönig, S. F. 2019, *ApJ*, 884, 171
- Hunt, L. K., Combes, F., García-Burillo, S., et al. 2008, *A&A*, 482, 133
- Imanishi, M., Nguyen, D. D., Wada, K., et al. 2020, *ApJ*, 902, 99
- Impellizzeri, C. M. V., Gallimore, J. F., Baum, S. A., et al. 2019, *ApJ*, 884, L28
- Izumi, T., Kohno, K., Fathi, K., et al. 2017, *ApJ*, 845, L5
- Izumi, T., Wada, K., Fukushige, R., Hamamura, S., & Kohno, K. 2018, *ApJ*, 867, 48
- Kalnajs, A. J. 1991, in *Dynamics of Disc Galaxies*, ed. B. Sundelius, 323
- Kormendy, J. & Ho, L. C. 2013, *ARA&A*, 51, 511
- Maloney, P. R. & Begelman, M. C. 1997, *ApJ*, 491, L43

Masters, K. L., Nichol, R. C., Hoyle, B., et al. 2011, MNRAS, 411, 2026
Mezcua, M. 2017, International Journal of Modern Physics D, 26, 1730021
Miller, J. M., Kaastra, J. S., Miller, M. C., et al. 2015, Nature, 526, 542
Miyamoto, Y., Nakai, N., Seta, M., et al. 2017, PASJ, 69, 83
Mortlock, D. J., Warren, S. J., Venemans, B. P., et al. 2011, Nature, 474, 616
Pringle, J. E. 1996, MNRAS, 281, 357
Renaud, F., Bournaud, F., Emsellem, E., et al. 2015, MNRAS, 454, 3299
Sanders, R. H. & Huntley, J. M. 1976, ApJ, 209, 53
Sassano, F., Capelo, P. R., Mayer, L., Schneider, R., & Valiante, R. 2023, MNRAS, 519, 1837
Schawinski, K., Dowlin, N., Thomas, D., Urry, C. M., & Edmondson, E. 2010, ApJ, 714, L108
Smajić, S., Moser, L., Eckart, A., et al. 2014, A&A, 567, A119
Tristram, K. R. W., Impellizzeri, C. M. V., Zhang, Z.-Y., et al. 2022, A&A, 664, A142
Venemans, B. P., Walter, F., Zschaechner, L., et al. 2016, ApJ, 816, 37
Vital, E., Libralato, M., Kremer, K., et al. 2023, MNRAS, 522, 5740
Vital, E. & Mamon, G. A. 2021, A&A, 646, A63
Yang, J., Wang, F., Fan, X., et al. 2020, ApJ, 897, L14